SSD-TR-90-54

AEROSPACE REPORT NO.
TR-0089(4530-04)-2

Ultrasonic Evaluation of SRMU Bondlines

Prepared by

E. C. JOHNSON, J. N. SCHURR, and G. F. HAWKINS
Materials Sciences Laboratory
Laboratory Operations

4 January 1991

Prepared for

SPACE SYSTEMS DIVISION
AIR FORCE SYSTEMS COMMAND
Los Angeles Air Force Base
P. O. Box 92960
Los Angeles, CA 90009-2960

Engineering and Technology Group

THE AEROSPACE CORPORATION
El Segundo, California

This report was submitted by The Aerospace Corporation, El Segundo, CA 90245-4691, under Contract No. F04701-88-C-0089 with the Space Systems Division, P.O. Box 92960, Los Angeles, CA 90009-2960. It was reviewed and approved for The Aerospace Corporation by S. Feuerstein, Director, Materials Sciences Laboratory. Captain Sanders was the project officer for the Mission-Oriented Investigation and Experimentation (MOIE) program.

This report has been reviewed by the Public Affairs Office (PAS) and is releasable to the National Technical Information Service (NTIS). At NTIS, it will be available to the general public, including foreign nationals.

This technical report has been reviewed and is approved for publication. Publication of this report does not constitute Air Force approval of the report's findings or conclusions. It is published only for the exchange and stimulation of ideas.

DAVID SANDERS, CAPT, USAF
MOIE Project Officer
SSD/CNSS

RAYMOND M. LEONG, MAJ, USAF
MOIE Program Manager
AFSTC/WCO OL-AB

UNCLASSIFIED

SECURITY CLASSIFICATION OF THIS PAGE

REPORT DOCUMENTATION PAGE

1a. REPORT SECURITY CLASSIFICATION Unclassified	1b. RESTRICTIVE MARKINGS
2a. SECURITY CLASSIFICATION AUTHORITY	3. DISTRIBUTION/AVAILABILITY OF REPORT Approved for public release; distribution unlimited.
2b. DECLASSIFICATION/DOWNGRADING SCHEDULE	
4. PERFORMING ORGANIZATION REPORT NUMBER(S) TR-0089(4530-04)-2	5. MONITORING ORGANIZATION REPORT NUMBER(S) SSD-TR-90-54
6a. NAME OF PERFORMING ORGANIZATION The Aerospace Corporation Laboratory Operations 6b. OFFICE SYMBOL *(If applicable)*	7a. NAME OF MONITORING ORGANIZATION Space Systems Division
6c. ADDRESS *(City, State, and ZIP Code)* El Segundo, CA 90245-4691	7b. ADDRESS *(City, State, and ZIP Code)* Los Angeles Air Force Base Los Angeles, CA 90009-2960
8a. NAME OF FUNDING/SPONSORING ORGANIZATION 8b. OFFICE SYMBOL *(If applicable)*	9. PROCUREMENT INSTRUMENT IDENTIFICATION NUMBER F04701-88-C-0089
8c. ADDRESS *(City, State, and ZIP Code)*	10. SOURCE OF FUNDING NUMBERS PROGRAM ELEMENT NO. / PROJECT NO. / TASK NO. / WORK UNIT ACCESSION NO.

11. TITLE *(Include Security Classification)*

Ultrasonic Evaluation of SRMU Bondlines

12. PERSONAL AUTHOR(S)

Johnson, Eric C.; Schurr, Juliet N.; and Hawkins, Gary F.

13a. TYPE OF REPORT	13b. TIME COVERED FROM ____ TO ____	14. DATE OF REPORT *(Year, Month, Day)*	15. PAGE COUNT
		1991 January 4	22

16. SUPPLEMENTARY NOTATION

17. COSATI CODES		
FIELD	GROUP	SUB-GROUP

18. SUBJECT TERMS *(Continue on reverse if necessary and identify by block number)*

NDE
Gr/Ep Composites
Pulse Echo
Ultrasonic Testing

19. ABSTRACT *(Continue on reverse if necessary and identify by block number)*

Pulse Echo (PE) ultrasonic evaluation of a Solid Rocket Motor Upgrade (SRMU) test sample was performed in our laboratory. The test sample contained simulated delaminations between both the Gr/Ep composite/insulator bondline and the insulator/inert propellant bondline. In this report, the acoustic properties of the SRMU component materials are used to construct a theoretical model for ultrasonic pulse propagation within the sample. The experimental results are then compared with the predictions from this model. This evaluation showed that PE ultrasonic inspection of the SRMU bondlines is feasible. In addition, several means for improving one's capability to detect disbonded regions are suggested.

20. DISTRIBUTION/AVAILABILITY OF ABSTRACT	21. ABSTRACT SECURITY CLASSIFICATION
☒ UNCLASSIFIED/UNLIMITED ☐ SAME AS RPT ☐ DTIC USERS	Unclassified
22a. NAME OF RESPONSIBLE INDIVIDUAL	22b. TELEPHONE *(Include Area Code)* / 22c. OFFICE SYMBOL

DD FORM 1473, 84 MAR

83 APR edition may be used until exhausted.
All other editions are obsolete

SECURITY CLASSIFICATION OF THIS PAGE

UNCLASSIFIED

ACKNOWLEDGMENT

The authors would like to acknowledge S. Sherman's assistance with the table preparations.

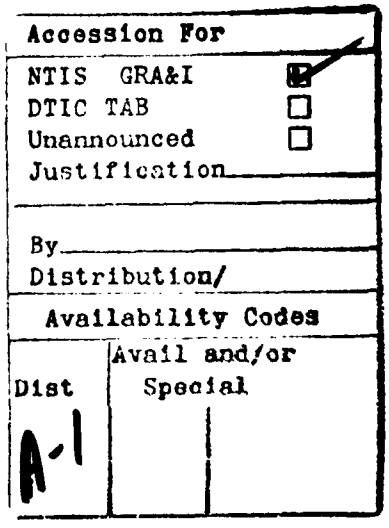

CONTENTS

FIGURES

TABLES

I. BACKGROUND

The Titan IV Solid Rocket Motor Upgrade (SRMU) motor case is composed of a graphite epoxy (Gr/Ep) composite as opposed to the steel used in earlier Titans. The inherent complexity of the Gr/Ep material presents new challenges for those performing nondestructive evaluation (NDE) of the solid rocket motor bondlines. Efforts to prove that a conventional ultrasonic pulse echo (PE) technique will work for this inspection have not been successful. The relative thickness of the composite case, coupled with the presence of multiple layers and porosity within the material, significantly lowers the signal-to-noise ratio for echoes reflected from the bondlines. The Aerospace Corporation was asked to render assistance in an effort to provide a "proof of concept" for the use of the PE technique. Samples were obtained from the contractor by Aerospace for this purpose. The results of the ultrasonic testing of one of these samples and the consequent development of a modified PE technique by the Materials Sciences Laboratory (MSL), Material Physics Section, are presented in this report.

II. SAMPLE DESCRIPTION

Figure 1 is a schematic (exploded view) of sample PTS-T-2B-6. This sample is representative of a portion of the SRMU cylindrical section and consists of three layers, Gr/Ep composite, 178A rubber insulator, and inert propellant. Note that the inert propellant layer of this sample is about 1.4 cm thick, whereas the actual propellant thickness of the SRMU is ~ 110 cm. As depicted, the sample was prepared with four purposely disbonded regions, two in the composite/insulator (C/I) bondline and two in the insulator/propellant (I/P) bondline. The disbonds in the left half of the sample, intended to represent the case where the disbonded surfaces are osculant (a "kissing" disbond), are simulated by a 5 mil thick Grafoil insert. The Grafoil is believed to permit a slight acoustic coupling across the interface. The disbonds in the right half of the sample, intended to emulate the case where there is a physical separation between the disbonded surfaces, are simulated by 11 mil thick "Teflon pillows." The Teflon pillows are composed of TX1040 bleed cloth which is sandwiched between 2–3 mil thick Teflon sheets.

Parameters which describe the acoustic properties of the materials that comprise the sample are listed in Table 1. These values were measured by the contractor at 0.5 MHz. The acoustic impedance, Z, is simply the product of the acoustic velocity and the density. The attenuation coefficient, α, permits one to determine the reduction in amplitude of the signal as it propagates through a given length, ℓ, of each medium.

Table 1. Acoustic Properties of Water and the SRMU Materials at 0.5 MHz

Medium	Density (g/cm^3)	AcousticVelocity (cm/s)	Acoustic Impedance $Z(g/cm^2 \cdot s)$	Attenuation Coeff. α (dB/cm)
Water (Medium 1)	1.0	1.5×10^5	1.5×10^5	0.0005
Gr/Ep Composite (Medium 2)	1.5	2.7×10^5	4.1×10^5	4.3
Insulator (Medium 3)	1.2	1.5×10^5	1.8×10^5	1.8
Propellant (Medium 4)	1.8	1.8×10^5	3.2×10^5	??

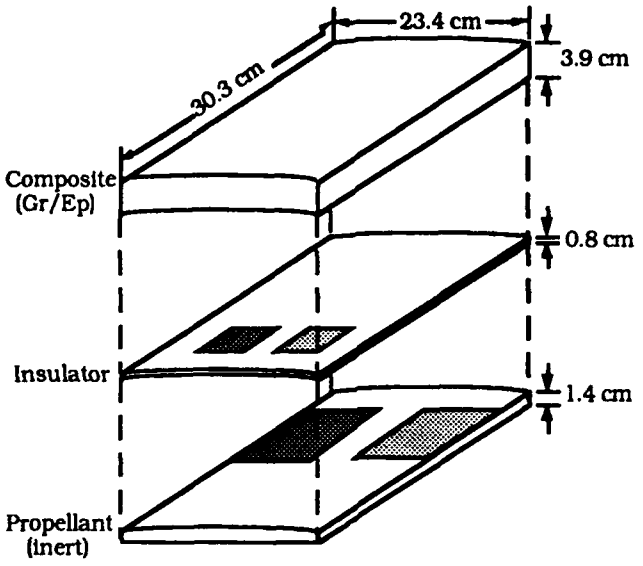

Fig. 1. Schematic of SRMU Sample PTS-T-2B-6. Top, middle, and bottom layers are Gr/Ep composite, 178 rubber insulator, and inert propellant, respectively. The shaded areas represent the Grafoil (left) and Teflon pillow (right) inserts placed in the composite/insulator (C/I) bondline and insulator/propellant (I/P) bondline to simulate disbonds. The inserts in the C/I bondline are 2 × 2 in., and the inserts in the I/P bondline are 3.5 × 4 in. in size.

III. THEORY

The geometry associated with an ultrasonic PE scan of the sample is depicted in Fig. 2. The drive pulse of amplitude D, which is generated by the transducer, propagates through the water (medium 1) to the sample composite surface (medium 2). A part of the drive pulse is transmitted into the composite while the rest is reflected back towards the transducer. The attenuation of the drive pulse by the water is negligible. The part of the drive pulse which is transmitted into the composite is attenuated by the composite before reaching the C/I bondline. At the bondline the ultrasonic pulse is again partially transmitted and reflected.

The Gr/Ep composite layer is relatively thick (3.9 cm) and the attenuation coefficient, α, is large. The amplitude of a 0.5 MHz signal passing through the Gr/Ep composite will be attenuated by $\alpha_2 \ell_2 = 16.3$ dB, i.e., reduced by a multiplicative factor of $M_2 = 0.14$, where the subscript 2 refers to medium 2. Thus, the signal amplitude is significantly reduced before it reaches the bondlines of interest. In addition, the echoes from these bondlines are reduced again by this same factor. Furthermore, due to the inherent porosity in the Gr/Ep composite, the attenuation across the composite can vary significantly. This variation, coupled with the small signal amplitude, results in a low signal-to-noise ratio which makes PE imaging of the bondlines very difficult.

The reflection and transmission coefficients which characterize the interface between two mediums (A and B) will be denoted by R_{AB} and T_{AB}, respectively. These coefficients can be computed using the well known equations

$$R_{AB} = \frac{Z_B - Z_A}{Z_A + Z_B} \text{ and } T_{AB} = \frac{2Z_B}{Z_A + Z_B}$$

where Z_A and Z_B are the acoustic impedances of medium A and B, respectively. Note that the subscripted coefficients are order specific, i.e., T_{AB}

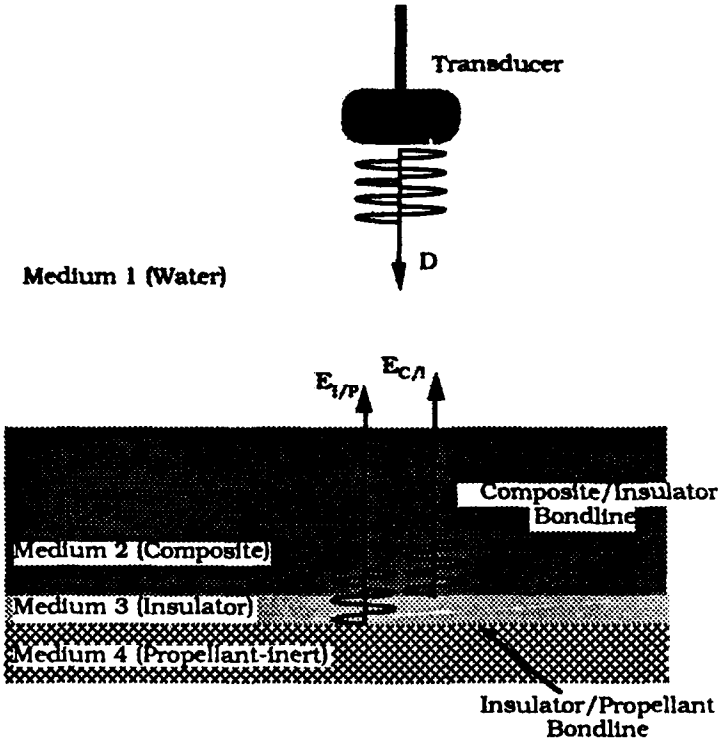

Fig. 2. Pulse Echo Scan Set-Up of the SRMU Sample

pertains to the case where sound propagates from medium A to medium B, whereas T_{BA} refers to the case where sound propagates from medium B to medium A. A negative R_{AB} value indicates that the pulse reverses phase upon reflection at the interface.

$E_{C/I}$ and $E_{I/P}$ will be used to represent the amplitude of the pulse echoes which return from the C/I bondline and the I/P bondline, respectively. A good bondline will reflect less sound than a bad bondline. Therefore, by monitoring the changes in $E_{C/I}$ and $E_{I/P}$, variations in these bondlines can be detected. $E_{C/I}$ and $E_{I/P}$ can be calculated using the following expressions:

$$E_{C/I} = D\{T_{12}R_{23}T_{21}(M_2)^2\} \text{ and } E_{I/P} = D\{T_{12}T_{23}R_{34}T_{32}T_{21}(M_2)^2(M_3)^2\}$$

where T_{AB}, R_{AB}, D, and M_A are defined above. The relevant T_{AB}, R_{AB}, M_A, and E values for cases where the layers are properly bonded; where there is a C/I disbond; and where there is an I/P disbond; were calculated, using the information from Table 1, and listed in Table 2. Note that in the case of a C/I disbond, $R_{23} = -1$ (assume total reflection) and $T_{23} = 0$. Similarly, for an I/P disbond, $R_{34} = -1$ and $T_{34} = 0$.

Table 2. Theoretical Echo Amplitude Values Calculated from Acoustic Property Values at 0.5 MHz

	Bonded		C/I Disbond		I/P Disbond	
	$E_{C/I}$	$E_{I/P}$	$E_{C/I}$	$E_{I/P}$	$E_{C/I}$	$E_{I/P}$
Echo Amplitude	**-0.0060D**	**0.0027D**	**-0.016D**	**0**	**-0.0060D**	**-0.010D**
T_{12}	1.5	1.5	1.5	1.5	1.5	1.5
T_{23}		0.62		0		0.62
R_{23}	-0.38		-1		-0.38	
R_{34}		0.27		0.27		-1
T_{32}		1.38		1.38		1.38
T_{21}	0.53	0.53	0.53	0.53	0.53	0.53
M_2	0.14	0.14	0.14	0.14	0.14	0.14
M_3		0.85		0.85		0.85

IV. ULTRASONIC A-SCAN AND C-SCAN TESTING

The PTS-T-2B-6 sample was coated with a thin plastic layer to prevent water from entering the sides of the sample. The sample was then submerged in a water tank for PE ultrasonic A-scan and C-scan testing.

A. A-SCANS

In an A-scan the ultrasonic data from a selected location on the sample are presented in the form of a scope trace with signal amplitude on the vertical axis and time on the horizontal axis. To generate the A-scan images, a flat, 1 in. diameter, 0.5 MHz lambda transducer (Ultran L100-0.5 #94708) was positioned 6.8 cm above the composite surface of the sample. 0.5 MHz toneburst pulses were used to drive the transducer, and the resultant signal was filtered using a 0.5 MHz bandpass filter. A-scans of three different locations from both the right and left side of the sample are shown in Fig. 3 and Fig. 4, respectively. The first echo in each trace comes from the reflection off the front surface of the sample. The echoes which follow are the result of reflection from the various interfaces in the sample. The C/I and I/P bondline echoes (labeled in the figures) can be recognized by their position in time relative to the echo from the front surface. The somewhat broadened echo, which follows the front surface echo and precedes the C/I bondline echo, results from a summation of reflections from the multiple interfaces within the composite itself.

In Fig. 3, the three A-scans from the right (Teflon pillow insert) side of the part are juxtaposed. Trace 3a corresponds to a location where both the C/I and I/P bondlines are well bonded, trace 3b to where there is a C/I disbond, and trace 3c to where there is an I/P disbond. Similar comments apply to A-scans from the left side (Grafoil insert) of the sample and are depicted in Fig. 4.

In Tables 3 and 4 parameters obtained from the A-scans of Figs. 3 and 4 are compared to the theoretical predictions of Table 2. Recall that ideal disbonds (i.e., resulting in a reflection coefficient of -1.0 and a transmission coefficient of 0) were assumed in the calculations which led

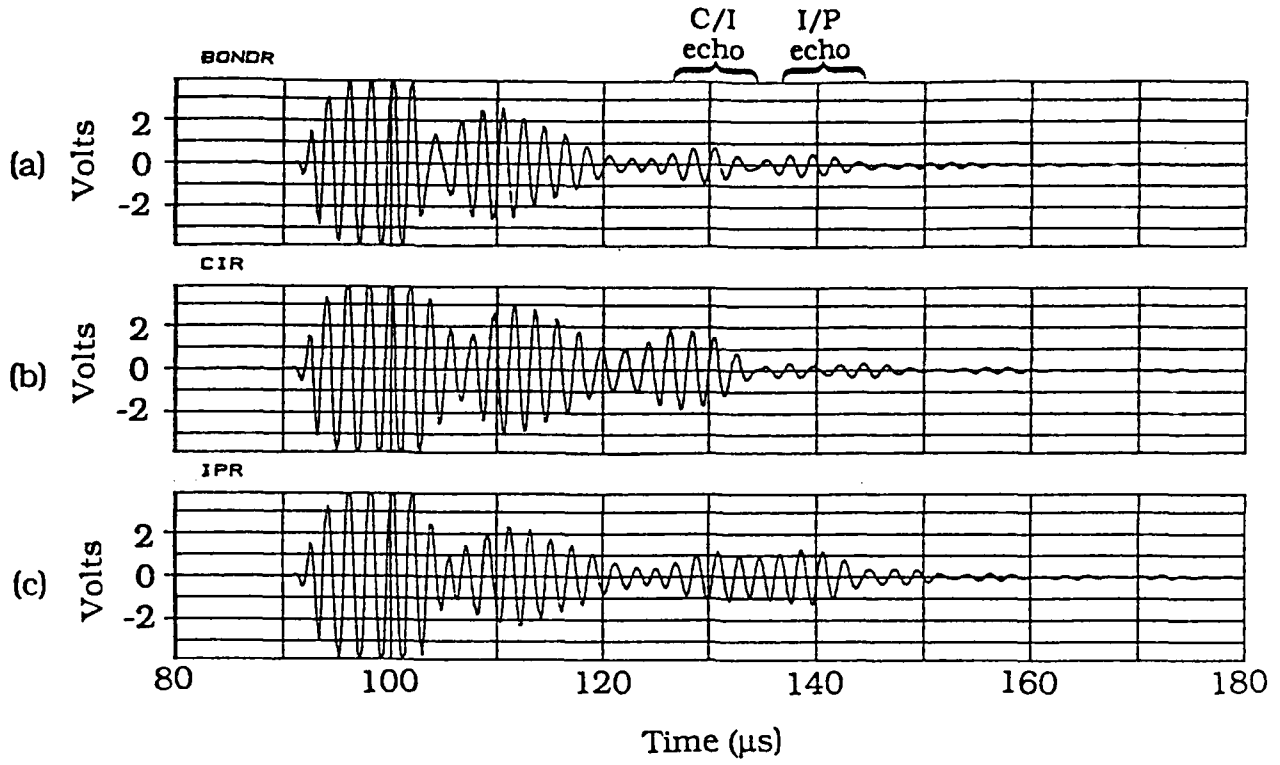

Fig. 3. 0.5 MHz A-Scans of SRMU PTS-T-2B-6 from the Right (Teflon) Side of the Sample. (a) bonded, (b) C/I disbonded, (c) I/P disbonded.

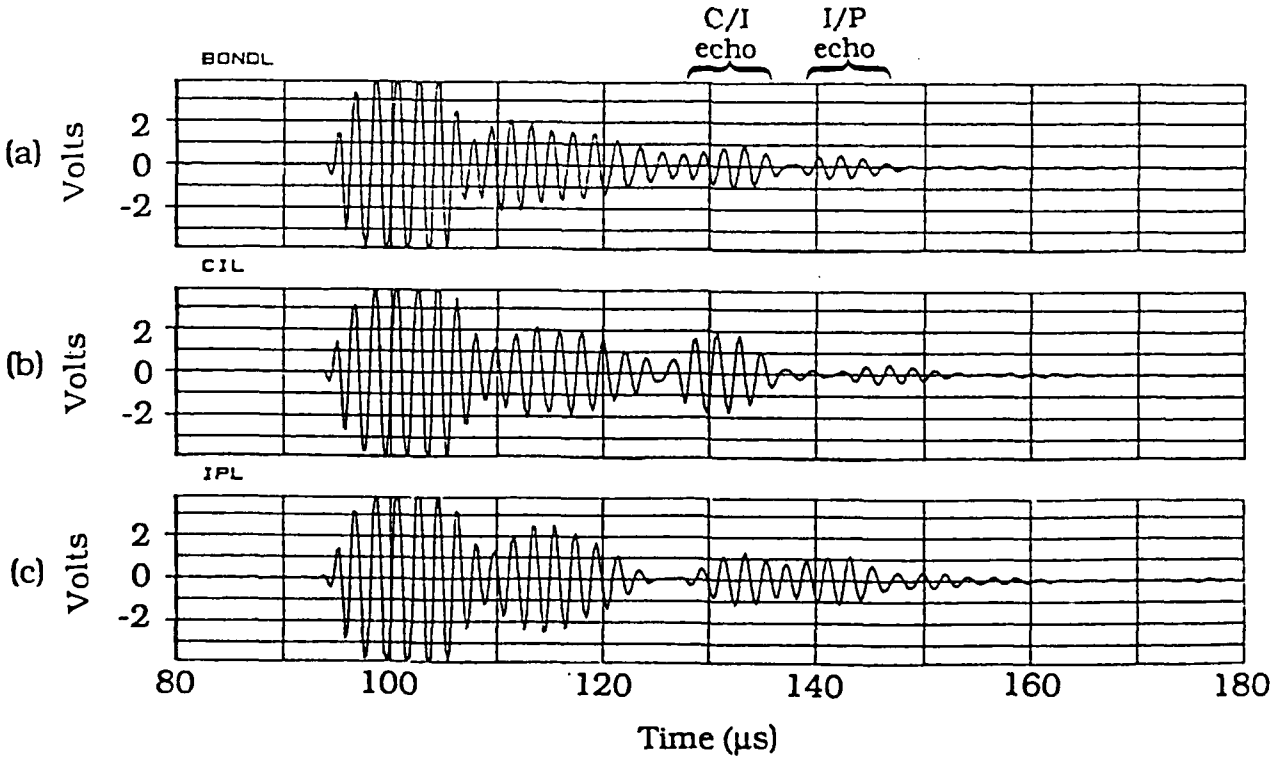

Fig. 4. 0.5 MHz A-Scans of SRMU PTS-T-2B-6 from the Left (Grafoil) Side of the Sample. (a) bonded, (b) C/I disbonded, (c) I/P disbonded.

Table 3. Comparison of Theoretical and Experimental (Teflon Side) Echo Amplitude Ratios

Right (Teflon) side of sample	$\frac{E_{I/P}}{E_{C/I}}$		$\frac{E_{C/I}}{E_{C/I}\text{(Bonded)}}$		$\frac{E_{I/P}}{E_{I/P}\text{(Bonded)}}$	
Trace No. (Location of A-scan)	Theor.	Exp.	Theor.	Exp.	Theor.	Exp.
Trace 3a (Bonded)	-0.45	-0.65	1	1	1	1
Trace 3b (C/I disbonded)	0	-0.17	2.5	2.3	0	0.60
Trace 3c (I/P disbonded)	1.6	1.0	1	1.5	-3.4	-2.4

Table 4. Comparison of Theoretical and Experimental (Grafoil Side) Echo Amplitude Ratios

Left (Grafoil) side of sample	$\frac{E_{I/P}}{E_{C/I}}$		$\frac{E_{C/I}}{E_{C/I}\text{(Bonded)}}$		$\frac{E_{I/P}}{E_{I/P}\text{(Bonded)}}$	
Trace No. (Location of A-scan)	Theor.	Exp.	Theor.	Exp.	Theor.	Exp.
Trace 4a (Bonded)	-0.45	-0.56	1	1	1	1
Trace 4b (C/I disbonded)	0	-0.11	2.5	2.0	0	0.40
Trace 4c (I/P disbonded)	1.6	0.88	1	1.3	-3.4	-2.1

to the predictions of Table 2. The disbonds in the samples, however, were not ideal (as was expected for the Grafoil). Sound leaked through both the Teflon and Grafoil inserts in the C/I bondline as evidenced by a nonzero $E_{I/P}$ value at these locations. The Teflon insert produces a slightly higher amplitude echo (greater reflection) than the Grafoil insert. In addition, the composite microstructure varies from point to point as can be seen by changes in the amplitude and phase of the broad echo which precedes the C/I echo. This variation serves to moderate the amount of sound which reaches the C/I and I/P interfaces.

With the above restrictions in mind, one notes that the $E_{C/I}$ and $E_{I/P}$ variations in the bonded and disbonded locations are in fair agreement with theory. For instance, a C/I disbond causes $E_{C/I}$ to increase by more than a factor of 2. One might also note the distinctive 180° phase shift (indicated by a negative sign) in the I/P echo which accompanies an I/P disbond.

B. C-SCANS

In a C-scan, the ultrasonic data are plotted as a function of the transducer position over the sample surface. Typically, the ultrasonic data are presented in the form of a color map where the color represents the signal amplitude at each position. For C-scan testing, a flat, 1.0 in. diameter, 0.5 MHz wideband transducer placed ~ 5 cm above the sample was used to perform the boustrophedonic scan. 0.5 and 0.3 MHz toneburst pulses were used to drive the transducer, and the resultant signals were bandpass filtered at the appropriate frequency. The C-scan data in Figs. 5a, 6a, and 7a were taken at 0.5 MHz, while the data in Figs. 5b, 6b, and 7b were taken at 0.3 MHz. All C-scan data are presented using a 0 to -18 dB scale, where the highest signal from the sample was established as the 0 dB reference.

In Fig. 5, the two C-scan images were generated by recording $E_{I/P}$ as a function of position. The I/P echo occurs approximately 40 μs after the front surface echo. In the 0.5 MHz scan, the I/P disbonds are outlined by the two rectangular areas of lower attenuation in the top half of the scan. (Refer to Fig. 1 for disbond locations.) The C/I disbond is not distinguishable from the bonded region. Recall that the 0.5 MHz A-scans in Figs. 3 and 4 also had indicated that $E_{I/P}$ would be large from the I/P disbonded region and small from both the bonded and C/I disbonded regions. In the 0.3 MHz scan, $E_{I/P}$ from both the C/I disbonded and I/P disbonded regions is attenuated to the same degree, i.e., 0 to -6 dB range. Although the disbonded regions can be distinguished from the bonded regions, one cannot tell whether the disbond is a C/I or I/P type. If one were to examine the 0.3 MHz RF signal, however, the phase of the I/P echo should reveal whether a C/I or I/P disbond was present. In both scans there appears to be a small disbonded area between the left and right I/P disbonds.

Figure 6 depicts the C-scan images generated when the C/I echo is peak detected over the sample. The C/I echo occurs ~ 30 μs after the front surface echo. Both scans show that only the area near the C/I disbond affected $E_{C/I}$ in contrast to the bonded region. Thus, by monitoring $E_{C/I}$,

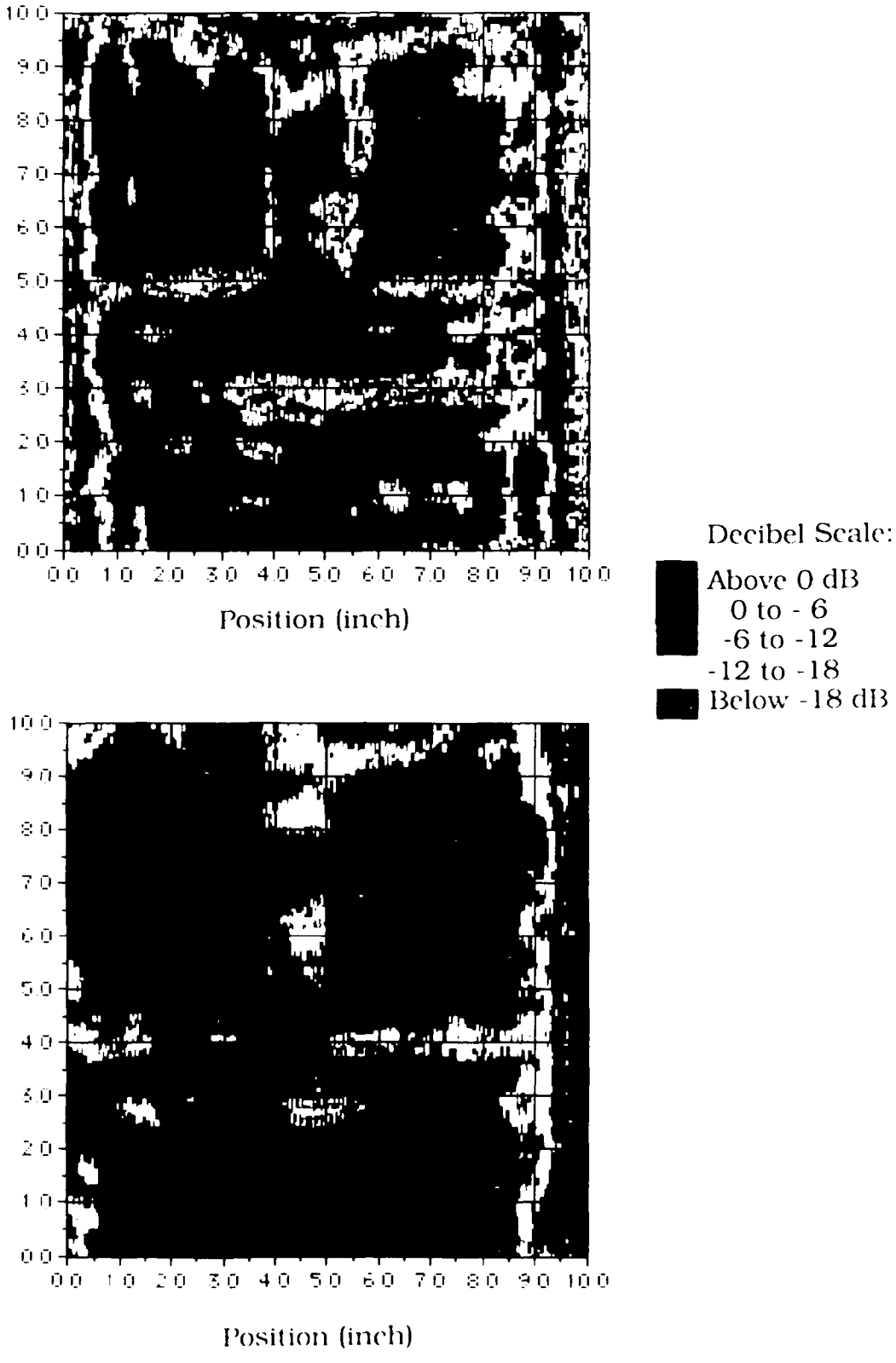

Fig. 5. C-Scans of SRMU PTS-T-2B-6. $E_{1,p}$ in dB vs position at (a) 0.5 MHz, and (b) 0.3 MHz.

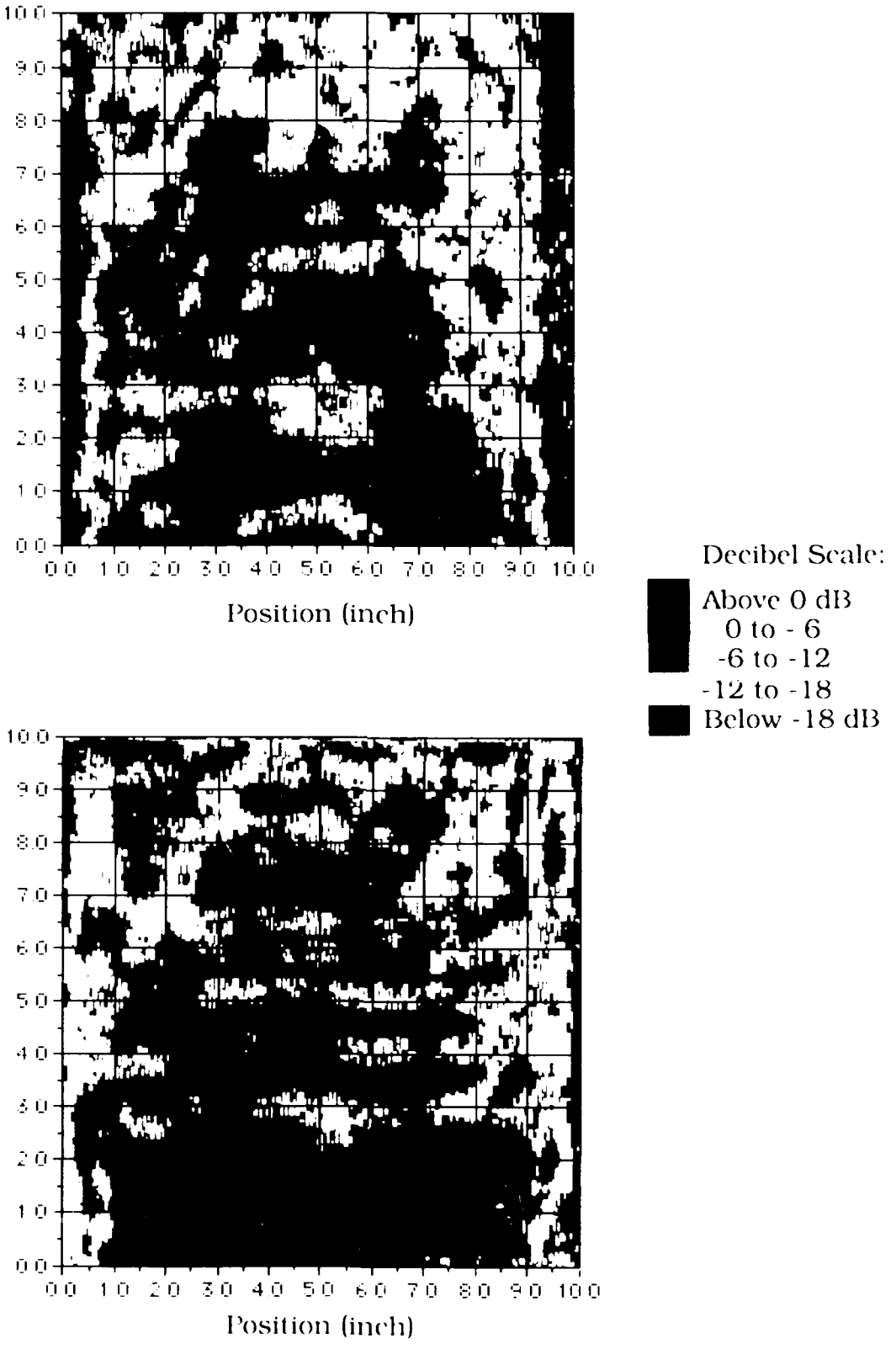

Fig. 6. C-Scans of SRMU PTS-T-2B-6. $E_{C,I}$ in dB vs position at (a) 0.5 MHz, and (b) 0.3 MHz.

the I/P disbonds could not be detected in the C-scan image. Again, the 0.5 MHz A-scans concur with the 0.5 MHz C-scan results. $E_{C/I}$ is large from the C/I disbonded region and similarly smaller from the bonded and I/P disbonded regions.

In an effort to improve the C-scan images of both the C/I and I/P disbonds, a technique that involved taking the ratio of certain echo amplitudes was implemented. Figure 7 shows the C-scan images where a ratio of $E_{I/P}$ to $E_{C/I}$ was recorded. In both the 0.5 and 0.3 MHz cases, not only is the magnitude of the $E_{I/P}$ to $E_{C/I}$ ratio affected by the disbonded region with respect to the bonded region, but the ratio magnitude is also dependent on the type of disbond being scanned. For example, in the 0.5 MHz scan, the ratio magnitude is highest over the I/P disbonds, lower over the bonded regions, and lowest over the C/I disbonds--as predicted and described previously in Tables 3 and 4. Thus, one can easily determine the location and type of disbond present in a sample. The 0.3 MHz scan is similar except that the lowest amplitudes are recorded for the bonded regions. Further study is required to address the differences between the 0.3 MHz and 0.5 MHz frequency results.

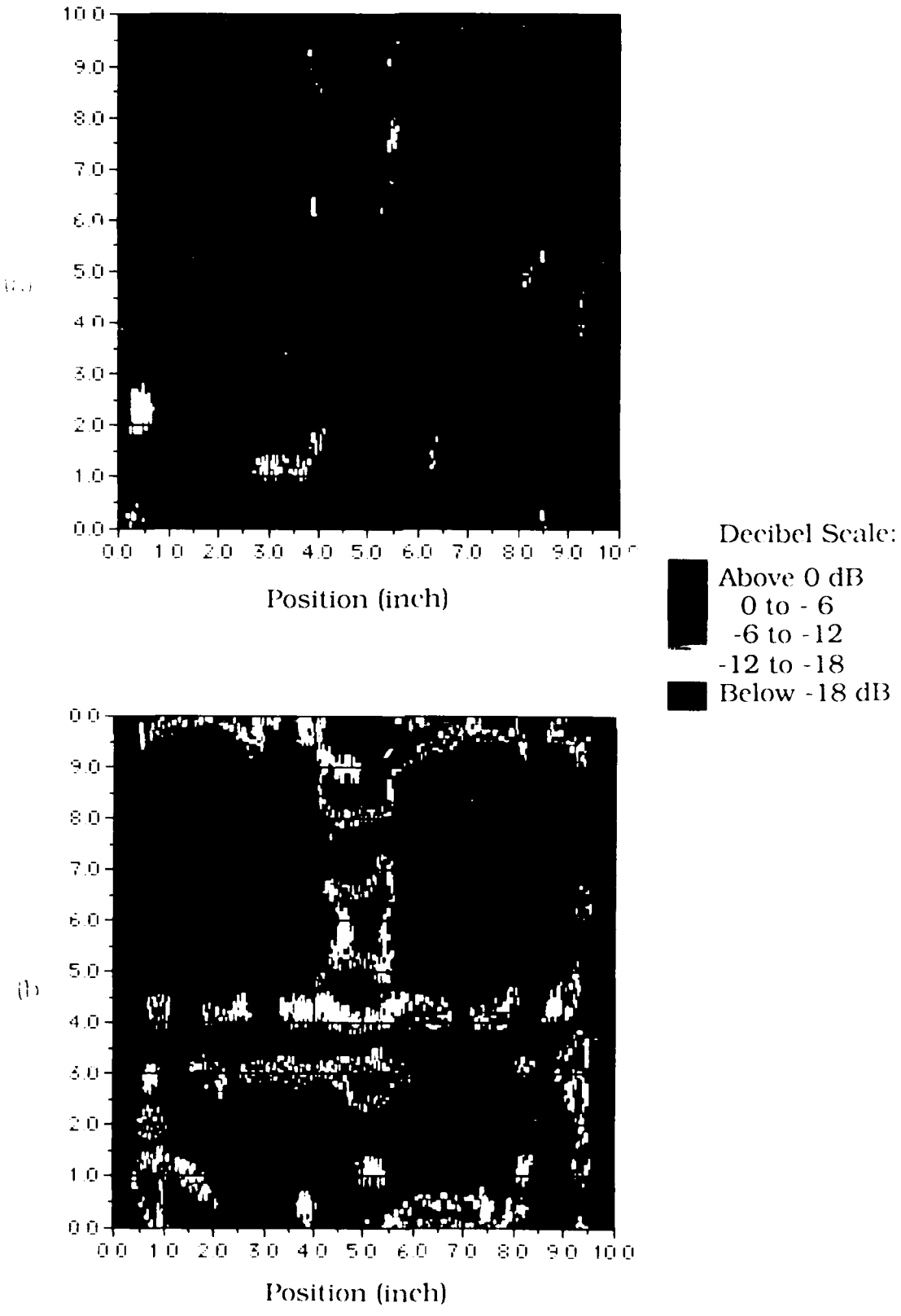

Fig. 7. C-Scans of SRMU PTS-T-2B-6. Ratio of $E_{I,P}$ to $E_{C,I}$ in dB vs position at (a) 0.5 MHz, and (b) 0.5 MHz.

V. DISCUSSION

The results of this study indicate that it is possible to perform ultrasonic inspection of the SRMU C/I and I/P bondlines using a modified PE technique. Conventional PE techniques, where echo amplitude information alone is recorded, do not adequately treat the low signal-to-noise problem.

To produce a more elucidative ultrasonic image, one needs to incorporate amplitude ratio or phase information of the echoes from both bondlines into the scan. Thus, if the RF waveform can be digitized at each point of the scan, one should be able to construct a signal processing algorithm to produce an optimal image of both bondlines.

It was also shown that the experimental echo amplitude measurements nearly followed the predictions calculated for a 5 MHz ultrasonic pulse propagating through our SRMU sample. Departures from the theoretical model may be accounted for by the fact that the sample did not have completely disbonded regions as the model assumed. Instead, Teflon and Grafoil inserts, which allowed some acoustic coupling, simulated the disbonds. In addition, while the model assumed uniform acoustic properties for the Gr/Ep composite, the inherent inhomegeneity of the composite material affected the ultrasonic pulse propagation in a manner dependent on the location on the sample.

Finally, it appears that there are advantages associated with scanning at lower frequencies, i.e., 0.5 MHz and below. However, this issue should be studied further to determine the best frequency for the SRMU material.

LABORATORY OPERATIONS

The Aerospace Corporation functions as an "architect-engineer" for national security projects, specializing in advanced military space systems. Providing research support, the corporation's Laboratory Operations conducts experimental and theoretical investigations that focus on the application of scientific and technical advances to such systems. Vital to the success of these investigations is the technical staff's wide-ranging expertise and its ability to stay current with new developments. This expertise is enhanced by a research program aimed at dealing with the many problems associated with rapidly evolving space systems. Contributing their capabilities to the research effort are these individual laboratories:

Aerophysics Laboratory: Launch vehicle and reentry fluid mechanics, heat transfer and flight dynamics; chemical and electric propulsion, propellant chemistry, chemical dynamics, environmental chemistry, trace detection; spacecraft structural mechanics, contamination, thermal and structural control; high temperature thermomechanics, gas kinetics and radiation; cw and pulsed chemical and excimer laser development, including chemical kinetics, spectroscopy, optical resonators, beam control, atmospheric propagation, laser effects and countermeasures.

Chemistry and Physics Laboratory: Atmospheric chemical reactions, atmospheric optics, light scattering, state-specific chemical reactions and radiative signatures of missile plumes, sensor out-of-field-of-view rejection, applied laser spectroscopy, laser chemistry, laser optoelectronics, solar cell physics, battery electrochemistry, space vacuum and radiation effects on materials, lubrication and surface phenomena, thermionic emission, photosensitive materials and detectors, atomic frequency standards, and environmental chemistry.

Electronics Research Laboratory: Microelectronics, solid-state device physics, compound semiconductors, radiation hardening; electro-optics, quantum electronics, solid-state lasers, optical propagation and communications; microwave semiconductor devices, microwave/millimeter wave measurements, diagnostics and radiometry, microwave/millimeter wave thermionic devices; atomic time and frequency standards; antennas, rf systems, electromagnetic propagation phenomena, space communication systems.

Materials Sciences Laboratory: Development of new materials: metals, alloys, ceramics, polymers and their composites, and new forms of carbon; nondestructive evaluation, component failure analysis and reliability; fracture mechanics and stress corrosion; analysis and evaluation of materials at cryogenic and elevated temperatures as well as in space and enemy-induced environments.

Space Sciences Laboratory: Magnetospheric, auroral and cosmic ray physics, wave-particle interactions, magnetospheric plasma waves; atmospheric and ionospheric physics, density and composition of the upper atmosphere, remote sensing using atmospheric radiation; solar physics, infrared astronomy, infrared signature analysis; effects of solar activity, magnetic storms and nuclear explosions on the earth's atmosphere, ionosphere and magnetosphere; effects of electromagnetic and particulate radiations on space systems; space instrumentation.